Cerâmica. 2025, v.71:eUZUG3814 http://dx.doi.org/10.1590/UZUG3814
ARTICLE

Spin-phonon coupling in $Ba_2Zn_2Fe_{12}O_{22}$ Y-type hexaferrite

F. M. Silva Júnior[1], C. W. Paschoal[2], M. C. Castro Junior[3]

[1]Instituto Federal de Educação, Ciência e Tecnologia do Maranhão, Departamento de Ensino, São José de Ribamar, MA, Brazil

[2]Universidade Federal do Ceará, Departamento de Física, Fortaleza, CE, Brazil

[3]Instituto Federal de Educação, Ciência e Tecnologia do Maranhão, Departamento de Ensino, Barreirinhas, MA, Brazil

Abstract

The spin-phonon coupling is frequently observed in magnetic materials and can be investigated using Raman spectroscopy. Surprisingly, there are no studies using Raman spectroscopy to confirm the existence of spin-phonon coupling in the Y-type Hexaferrite $Ba_2Zn_2Fe_{12}O_{22}$ (Zn_2Y), despite its ferrimagnetic nature. In this context, this paper aims to fill this gap. Raman spectra of Zn_2Y were measured from 296 K to 438 K, and a hardening of the mode at 660 cm^{-1} was observed near the Curie temperature. This behavior was associated with spin-phonon coupling.

Keywords: Spin-phonon coupling. Hexaferrite. Raman spectroscopy.

INTRODUCTION

The hexaferrite, discovered in the 1950s [1], can be described as a stacking of a sequence of three basic blocks: block S ($Me^{2+}Fe_4O_8$; spinel block, where Me denotes a divalent metal ion such as Fe^{2+}, Mg^{2+}, Zn^{2+}, Co^{2+}, etc.); block R $[(Ba, Sr)Fe_2O_{11}]^{2-}$; and block T $[(Ba, Sr)_3Fe_8O_{14}]$. Hexagonal ferrites have been classified according to their structure and composition into several classes, including M-type ($(Ba, Sr)Fe_{12}O_{19}$), W-type ($(Ba, Sr)Me_2Fe_{16}O_{27}$), Y-type ($(Ba, Sr)_2Me_2Fe_{12}O_{22}$), X-type ($(Ba, Sr)_2Me_2Fe_{28}O_{46}$), and Z-type ($(Ba, Sr)_2Me_2Fe_{24}O_{41}$) [2]. Among the Y-type hexaferrites, attention has been focused on Zn-based Y-type hexaferrite ($Ba_2Zn_2Fe_{12}O_{22}$ or Zn_2Y) due to its low insertion loss, wide bandwidth, low biasing field, and high anisotropy field (HA) for microwave device applications [3].

Contrary to $Ba_2Mg_2Fe_{12}O_{22}$, in which Mg is distributed in the octahedral and tetrahedral sites [4] in the $Ba_2Zn_2Fe_{12}O_{22}$, zinc is only in two different tetrahedral sites [5]. Zn_2Y hexagonal planar ferrite in that it has an easy plane of magnetization perpendicular to the c axis [5]. This compound is trigonal (space group $R\bar{3}m$); expressed in the hexagonal axes, the cell parameters are: a = b = 5.875(l) Å and c = 43.571(6) Å. Zn_2Y has three unit cells per unit formula (Z=3). Its magnetic structure is characterized by alternate stacks of L blocks and S blocks along c. Within each block, the magnetic moments of Fe^{3+} (S=5/2) are ferrimagnetically coupled and collinearly aligned in the ab plane. This yields a large magnetic moment on the L block and a small magnetic moment on the S block [1, 2].

Spin-phonon coupling plays a crucial role in hexaferrites, as it is associated with the magnetodielectric effect in Z-type hexaferrites [6]. However, spin-phonon coupling is frequently investigated and observed in magnetic compounds [7-11]. Despite its well-documented ferrimagnetic behavior (T_C = 403 K) [1, 12], spin-phonon coupling studies in Zn_2Y, as well as its temperature-dependent phonon spectra, have not been reported in the literature. One of the most employed techniques for investigating spin-phonon coupling is Raman spectroscopy. There have been few studies on the Raman spectroscopy of the Y-type hexaferrite Zn_2Y, except for some investigations involving the isostructural compounds: $Ba_{0.5}Sr_{1.5}Zn_2Fe_{12}O_{22}$ [13], $Ba_2Mg_2Fe_{12}O_{22}$ [14] and $BaSrCoZnFe_{11}AlO_{22}$ [15]. This paper aims to investigate spin-phonon coupling in the Zn_2Y hexaferrite and discuss its temperature-dependent vibrational properties.

EXPERIMENTAL

$Ba_2Zn_2Fe_{12}O_{22}$ (Zn_2Y) was prepared using the solid-state reaction method according to a stoichiometric mixture of $BaCO_3$, ZnO, and Fe_2O_3. The starting materials were mixed according to their molecular weight proportions and ground in an agate mortar, then sieved to obtain a homogeneous powder. The mixed powders were calcined at 1200 °C in the atmosphere for 8 hours. The resulting powders were investigated by X-ray diffraction (XRD) at room temperature using a Bruker D8 Advance powder diffractometer with Cu-Kα radiation (40 kV, 40 mA) in a 15° to 80° range with a step size of 0.02°. The X-ray diffraction pattern of the powders was compared with data from the ICSD (Inorganic Crystal Structure Database, FIZ Karlsruhe, and NIST) from the international diffraction database (ICSD#14239), confirming the formation of the Zn_2Y phase.

For the Raman spectroscopy measurements, the polycrystalline powder was uniaxially compressed into 7 mm pellets at 4 metric tons. The pellets were placed in alumina crucibles with sacrificial powder of the same composition and sintered in air at 1200°C for 16 hours to obtain dense ceramics. The Raman spectroscopy measurements were carried out using a Horiba iHR550 Raman spectrometer coupled with an Olympus BX41 microscope, equipped with a long working distance objective (20x, 20.5 mm). The 662 nm line from a diode laser operating at 17 mW was used

**flavio.junior@ifma.edu.br*
https://orcid.org/0009-0000-6578-4801

to excite the Raman signal, which was collected by an air-cooled Synapse CCD. High temperature measurements were performed by furnace TS 1200 LIKAM model in the range 296 K to 438 K.

RESULTS AND DISCUSSIONS

Figure 1 shows the XRPD pattern of the Zn_2Y sample. The experimental data was refined using the software GSAS. The X-ray diffraction pattern of the powders was compared with data from the ICSD (Inorganic Crystal Structure Database, FIZ Karlsruhe, and NIST) from the international diffraction database (ICSD#14239), confirming the formation of the Zn_2 Y phase. Additionally, the diffraction pattern indicated a small amount of $ZnFe_2O_4$ (3.3%) and $BaFe_2O_4$ (3.0%) as residual phase. These secondary phases are commonly observed in the synthesis of Zn_2Y hexaferrite [1].

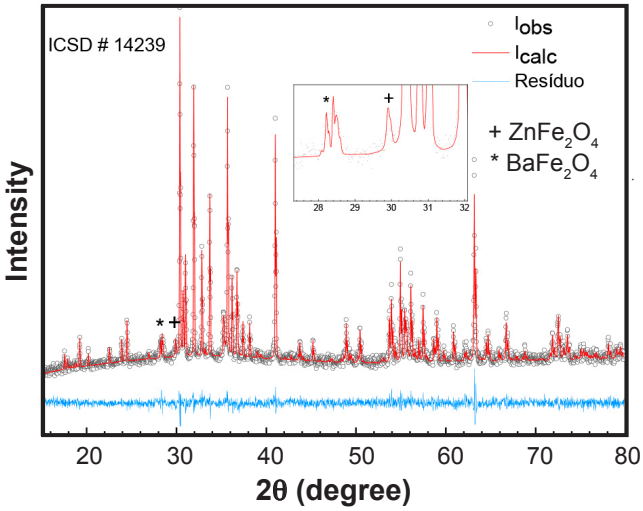

Figure 1: Observed, calculated, and diference XRPD profiles for Zn_2Y at room temperature. The low-intensity peaks identified with the cross and the asterisk represent the subphases $ZnFe_2O_4$ and $BaFe_2O_4$, respectively. These peaks are shown in an enlarged view in the inset.

Figure 2a shows the Raman spectrum at room temperature corresponding to the Zn_2Y sample. Group theory predicts 32 Raman-active phonons in Zn_2 Y, with their distribution in the irreducible representations of the $R\bar{3}m$ factor group being 14 A_{1g} + 18 E_g [16]. We observe sixteen modes at room temperature at the following wavenumbers: 723, 697, 660, 494, 461, 425, 385, 360, 330, 289, 280, 254, 221, 188, 174, 660and 130 cm^{-1}. Figures 2b and 2c show the evolution of the phonon spectra with increasing temperature. As we can see, except for the expected broadening of the bands due to anharmonic effects, there is no significant change in the spectra with increasing temperature, allowing us to rule out a structural phase transition in Zn_2Y within the investigated temperature range.

The symmetries of the main bands can be elucidated by comparing them with the Raman spectra of the isostructural compound $Ba_{0.5}Sr_{1.5}Zn_2Fe_{12}O_{22}$ [13], which allows us to conclude that in Zn_2Y, the bands at 697, 657, 494, 461, 360, and

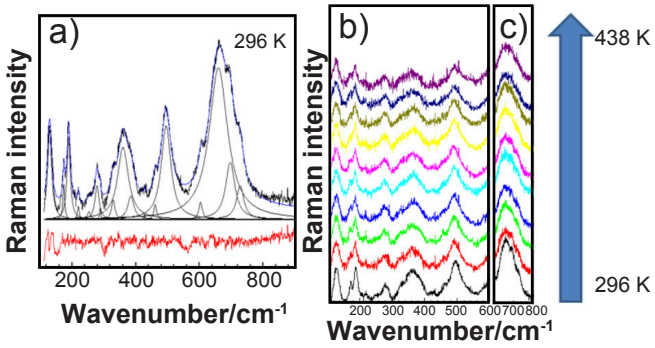

Figure 2: (a) Zn_2Y spectrum collected at room temperature. Temperature-dependent evolution of the Zn_2Y phonons: (b) low wavenumber (c) high wavenumber.

188 cm^{-1} are A_{1g}, while the bands at 289, 174, and 130 cm^{-1} are E_g. Regarding the classification of the bands, this task is quite complicated for Zn_2Y due to its complex crystal structure. It has tetrahedral and octahedral sites, in addition to the MeO_6 groups forming chains that share faces and edges, making it very difficult to assign the corresponding vibration modes to specific sites. Despite this, we can qualitatively classify some of these modes by considering the crystal structure of Zn_2Y, which is formed by octahedral FeO_6 and tetrahedral FeO_4 groups. In this context, classification can be done by comparing the Raman spectrum of Zn_2Y with that of magnetoplumbite ($BaFe_{12}O_{19}$) [17] and spinel-type ferrites [18, 19], which are materials that have octahedral and tetrahedral groups in their structures. It is known from the literature that ferrites (AFe_2O_4, where A is a divalent cation) are characterized by A_{1g} bands in the 660-720 cm^{-1} region, regardless of the nature of the divalent ion [18], which are related to the stretching of $Fe^{3+}O_4$ tetrahedra.

Additionally, studies show that the A_{1g} modes in the 460-640 cm^{-1} region [17] in ferrites with a normal spinel structure are dominated by $Fe^{3+}O_6$ octahedra. Thus, we suggest that the bands at 697 and 660 cm^{-1} present in Zn_2Y are associated with the vibrations of the MeO_4 tetrahedra in the S and T blocks (with Me = $p_{Zn}Zn^{2+}$ + (1-p_{Zn}) Fe^{3+}, where p_{Zn} is the population of zinc ions). While the modes at 494, 461, 360, 289, and 188 cm^{-1} are due to the vibration of the MeO_6 octahedron and the vibration of the O-Me-O bonds, respectively, the low-frequency bands are often associated with heavy cations. Therefore, we assign the mode at 130 cm^{-1} to Ba-O vibrations. Finally, the band at 174 cm^{-1} can be attributed to the vibrations of the entire S block, as it is in this region that the modes for the S block are found in spinel ferrites [17]. The classification of these modes is summarized in Table I.

Figure 3 shows the dependence of the position of the most intense mode at 660 cm^{-1} as a function of temperature, obtained through a fitting process. It is observed that, up to the Curie temperature (403 K), the phonon wavenumbers decrease. As observed, near this temperature, an anomaly occurs in the position of this active Raman mode. This happens because, at room temperature, Zn_2Y is ferrimagnetic, which leads to a contribution from the interactions between the Fe^{3+} - O - Fe^{3+}

Table I – Assignment of the main Raman-active modes observed in Zn_2Y.

Wavenumber (cm^{-1})	Symmetry	Assignment
697	A_{1g}	Stretching MeO_4
660	A_{1g}	Stretching MeO_4
494	A_{1g}	Stretching MeO_6
461	A_{1g}	Stretching MeO_6
360	A_{1g}	Vibration MeO_6
289	E_g	Vibration MeO_6
188	A_{1g}	O-Me-O bridge
174	E_g	Whole spinel block
130	E_g	Vibration Ba-O

magnetic ions in the phonon dependence on temperature, in addition to anharmonicity [20]. The deviation at the Curie temperature indicates that there is spin-phonon coupling in Zn_2Y. It is known from the literature that this coupling can be interpreted as a modulation of the exchange integral by phonons, which leads to a renormalization of the phonon. The spin-phonon contribution ($\Delta\omega_{s\text{-}ph}$) to the phonon frequency variation due to magnetic ordering can be written as [20, 21, 22]:

$$\Delta\omega_{s\text{-}ph} = \rho < \vec{S}_i . \vec{S}_j > \quad (1)$$

where ρ is the spin-phonon coupling constant and $<\vec{S}_i.\vec{S}_j>$ is the scalar spin correlation function. In the case of a ferrimagnetic material, ρ and $<\vec{S}_i.\vec{S}_j>$ are negative. As the temperature increases, the spin-phonon coupling is suppressed, since thermal agitation hinders magnetic ordering, and thus anharmonicity becomes more important at higher temperatures. With the spin-phonon coupling no longer existing, a change in the slope of the curve of the mode position at 660 cm^{-1} is expected at the Curie temperature. The contribution of the subphases $ZnFe_2O_4$ and $BaFe_2O_4$ to the observed anomaly can be readily dismissed, as the Néel temperatures of these ferrites are 10 K [23] and 227 K [24], respectively.

A similar result is found for $BiFeO_3$ [25], where there is softening and hardening for the A_1 and E modes, respectively, above the Néel temperature (643 K). F. M. Silva Júnior and C. W. A. Paschoal [26] observed spin-phonon coupling at the Curie temperature of BaM (723 K). M. A.P. Buzinaro, et al. [27] also observed the spin-phonon coupling at the Curie temperature (T_c = 720 K) of the M-type $SrFe_{12}O_{19}$ hexaferrite. Y.P. Santos et al. [28] observed strong spin-phonon coupling in the Z-type hexaferrite $Ba_{1.6}Sr_{1.4}Co_2Fe_{24}O_{41}$ using Raman spectroscopy, related to three magnetic transitions: conical-planar, uniaxial planar, and ferromagnetic-paramagnetic. Similarly to this work, these authors observed the spin-phonon coupling in the most intense Raman band associated with the stretching vibration of the FeO_4 tetrahedra. Finally, Raju et al. [29] also observed spin-phonon coupling in the

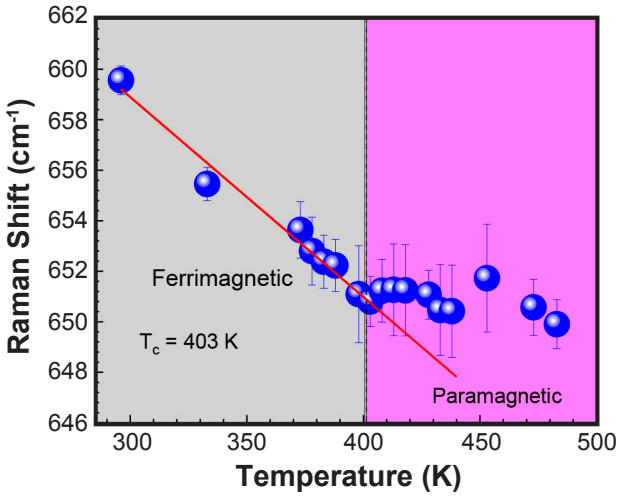

Figure 3: Temperature dependence of the Raman - active mode at 660 cm^{-1}. The dots represent the data points with error bars and the dashed line indicates the temperature at which the abnormality occurs. The continuous curve is a guide to the eyes

$SrFe_8Co_2Ti_2O_{19}$ hexaferrite at 330 K, which they attributed to a magnetic transition from a collinear phase to a conical phase [1]. All spin-phonon couplings in these hexaferrites were observed in modes with A_{1g} symmetry. These results support our hypothesis of spin-phonon coupling in Zn_2Y in the high-temperature regime.

CONCLUSION

The Y-type hexaferrite $Ba_2Zn_2Fe_{12}O_{22}$ was obtained successfully by solid state reaction. The transition from the ferrimagnetic to the paramagnetic phase, which occurs at 403 K, is reflected in the temperature dependence of the phonon observed near 660 cm^{-1}. Its frequency increases abruptly above Tc due to spin-phonon coupling.

ACKNOWLEDGMENTS

The authors acknowledge the financial support of the funding agencies CAPES, CNPq, and FAPEMA.

REFERENCES

[1] Pullar RC. Hexagonal ferrites: A review of the synthesis, properties and applications of hexaferrite ceramics. *Prog Mater Sci.* 2012;**57**:1191–334. doi:10.1016/j.pmatsci.2012.04.001.

[2] Kimura T. Magnetoelectric hexaferrites. *Annu Rev Condens Matter Phys.* 2012;**3**:93–110. doi:10.1146/annurev-conmatphys-020911-125101.

[3] Jalli J, Hong YK, Bae S, Lee JJ, Abo GS, Park JH, et al. Magnetic and microwave properties of ferrimagnetic Zr-substituted $Ba_2Zn_2Fe_{12}O_{22}$ (Zn-Y) single crystals. *J Appl Phys.* 2011;**109**. doi:10.1063/1.3560885.

[4] Collomb A, Muller J, Fournier T. Magnesium location in the barium-magnesium-iron Y-type hexagonal ferrite. *Mater*

Res Bull. 1993;**28**. doi:10.1016/0025-5408(93)90105-m.
[5] Collomb A, Muller J, Guitel JC, Desvignes JM. Crystal structure and zinc location in the $BaZn_2Fe_{12}O_{22}$ Y-type hexagonal ferrite. *J Magn Magn Mater.* 1989;**78**. doi:10.1016/0304-8853(89)90089-9.
[6] Zhang X, Zhao YG, Cui YF, Ye LD, Wang JW, Zhang S, et al. Magnetodielectric effect in Z-type hexaferrite. *Appl Phys Lett.* 2012;**100**. doi:10.1063/1.3677672.
[7] Bhadram VS, Rajeswaran B, Sundaresan A, Narayana C. Spin-phonon coupling in multiferroic $RCrO_3$ (R=Y, Lu, Gd, Eu, Sm): A Raman study. *EPL.* 2013;**101**:17008. doi:10.1209/0295-5075/101/17008.
[8] Kumar D, Kumar S, Sathe VG. Spin-phonon coupling in ordered double perovskites A_2CoMnO_6 (A=La, Pr, Nd) probed by micro-Raman spectroscopy. *Solid State Commun.* 2014;**194**:59–64. doi:10.1016/j.ssc.2014.06.017.
[9] Mochizuki M, Furukawa N, Nagaosa N. Theory of spin-phonon coupling in multiferroic manganese perovskites $RMnO_3$. *Phys Rev B.* 2011;**84**:144409. doi:10.1103/PhysRevB.84.144409.
[10] Bezerra R, Filho M, Ayala AP, William C, Paschoal A. Spin-phonon coupling in Y_2NiMnO_6 double perovskite probed by Raman spectroscopy. *J Appl Phys.* 2013. doi:10.1063/1.4804988.
[11] Ferreira WS, Moreira JA, Almeida A, Chaves MR, Araújo JP, Oliveira JB, et al. Spin-phonon coupling and magnetoelectric properties: $EuMnO_3$ versus $GdMnO_3$. *Phys Rev B.* 2009;**79**:054303. doi:10.1103/PhysRevB.79.054303.
[12] Verweel J. Magnetic properties of ferrite single crystals with the Y structure. *J Appl Phys.* 1967;**38**(3):1111–7. doi:10.1063/1.1709506.
[13] Kamba S, et al. Dielectric, magnetic, and lattice dynamics properties of Y-type hexaferrite $Ba_{0.5}Sr_{1.5}Zn_2Fe_{12}O_{22}$: Comparison of ceramics and single crystals. *J Appl Phys.* 2010;**107**(10). doi:10.1063/1.3402379.
[14] Khanduri H, Dimri MC, Kooskora H, Heinmaa I, Viola G, Ning H, et al. Structural, dielectric, magnetic, and nuclear magnetic resonance studies of multiferroic Y-type hexaferrites. *J Appl Phys.* 2012;**112**. doi:10.1063/1.4754532.
[15] Kamba S, Borodavka F, Kadlec F, Kadlec C, Chai YS, Zhai K, et al. Vibrational spectra of multiferroics with Y- and Z-type hexaferrite structures. *Ferroelectrics.* 2018;**532**:208–20. doi:10.1080/00150193.2018.1499406.
[16] Rousseau DL, Bauman RP, Porto SPS. Normal mode determination in crystals. *J Raman Spectrosc.* 1981;**10**:253–90. doi:10.1002/jrs.1250100152.
[17] Kreisel J, Lucazeau G, Vincent H. Raman spectra and vibrational analysis of $BaFe_{12}O_{19}$ hexagonal ferrite. *J Solid State Chem.* 1998;**137**. doi:10.1006/jssc.1997.7737.
[18] Degiorgi L, Blatter-Mörke I, Wachter P. Magnetite: Phonon modes and the Verwey transition. *Phys Rev B.* 1987;**35**(11):5421. doi:10.1103/PhysRevB.35.5421.
[19] McCarty KF, Boehme DR. A Raman study of the systems $Fe_{3-x}Cr_xO_x$ and $Fe_{2-x}Cr_xO_3$. *J Solid State Chem.* 1989;**79**(1):19–27. doi:10.1016/0022-4596(89)90245-4.
[20] Lockwood DJ, Cottam MG. The spin-phonon interaction in FeF_2 and MnF_2 studied by Raman spectroscopy. *J Appl Phys.* 1988;**64**:5876–8. doi:10.1063/1.342186.
[21] Baltensperger W, Helman JS. Extraction studies of antimony bromide into benzene. *Helv Phys Acta.* 1968;**41**:668. doi:10.1016/s0003-2670(01)80355-x.
[22] Balkanski M, Wallis RF, Haro E. Anharmonic effects in light scattering due to optical phonons in silicon. *Phys Rev B.* 1983;**28**:1928–34. doi:10.1103/PhysRevB.28.1928.
[23] Goya GF, Rechenberg HR. Ionic disorder and Néel temperature in $ZnFe_2O_4$ nanoparticles. *J Magn Magn Mater.* 1999;**196**:191–2. doi:10.1016/s0304-8853(98)00723-9.
[24] Melzer K, et al. Magnetic properties of barium monoferrite. *Cryst Res Technol.* 1989;**24**(1):K9–K12. doi:10.1002/crat.2170240126.
[25] Rovillain P, Cazayous M, Gallais Y, Sacuto A, Lobo RPSM, Lebeugle D, et al. Polar phonons and spin excitations coupling in multiferroic $BiFeO_3$ crystals. *Phys Rev B.* 2009;**79**:180411. doi:10.1103/PhysRevB.79.180411.
[26] Silva Júnior FM, Paschoal CWA. Spin-phonon coupling in $BaFe_{12}O_{19}$ M-type hexaferrite. *J Appl Phys.* 2014;**116**. doi:10.1063/1.4904062.
[27] Buzinaro MAP, Macêdo MA, Costa BFO, Ferreira NS. Disorder of Fe_2O_5 bipyramids and spin-phonon coupling in $SrFe_{12}O_{19}$ nanoparticles. *Ceram Int.* 2019;**45**:13571–4. doi:10.1016/j.ceramint.2019.05.129.
[28] Santos YP, Andrade BC, Machado R, Macêdo MA. Spin–phonon coupling in multiferroic $Ba_{1.6}Sr_{1.4}Co_2Fe_{24}O_{41}$. *J Magn Magn Mater.* 2014;**364**:95–7. doi:10.1016/j.jmmm.2014.03.079.
[29] Raju N, Kumar KU, Reddy MS, Reddy GR, Reddy YP, Reddy VR. Magnetic and spin-phonon coupling studies of magneto-electric $SrFe_8Co_2Ti_2O_{19}$ M-type hexaferrite. *J Magn Magn Mater.* 2022;**562**:169868. doi:10.1016/j.jmmm.2022.169868.

(Rec. 31-Jan-2025, Rev. 24-Mar-2025, Ac. 14-Apr-2025)
(AE: Daniel Z. de Florio)